Polarimetry and Spectroscopy on Geostationary Satellites with the Nordic Optical Telescope

Semeli Papadogiannakis, Torbjörn Sundberg, Per Hägg
Swedish Defence Research Agency
Hanna Sundberg
Swedish Space Corporation

ABSTRACT

We present new polarimetry and spectroscopy data from the 2.56 meter Nordic Optical Telescope for three geostationary satellites. The aim was to examine whether polarization and spectra can be used for characterization and identification of satellites and to study the reddening effect in the spectra possibly linked to space exposure.

We found a strong dependency between the degree of polarization and the phase angle that is individual for each satellite, with polarization variations as large as 25% for certain phase angles. We also found spectroscopic differences but their origin is unclear. In conclusion we find that a wide range of phase angles need to be probed for characterization both using polarimetry and spectroscopy.

1. INTRODUCTION AND BACKGROUND

Characterization and classification of resident space objects (RSOs) becomes increasingly important as we have seen a sharp rise in the number of objects in orbit in the last few years. Characterization measurements can be used for object identification, operational status and geometry among other things and is of interest for a wide variety of sectors including military (e.g. threat assessment), political (e.g., treaty compliance) and research (e.g., material science). Characterization also is part of space situational awareness (SSA) and space domain awareness (SDA) which is a priority for many space faring nations [1].

Non-resolved object characterization can be done in many different ways. The most common is to study light-curves at different phase angles (e.g. [2]), often in conjunction with machine learning methods (e.g. [3] [4]). In this paper we are looking into the possibility of using polarimetry and medium resolution spectroscopy for this purpose on geostationary (GEO) satellites.

Spectroscopy measurements of RSOs, have been used for characterization purposes (e.g. [5], [6], [7], [9], [10]). In one case [11], spectroscopic measurements in orbit have been compared to laboratory measurements of the same object. A "reddening" effect on the spectra has frequently been reported (e.g. [12]), in which the peak of reflectance increases with wavelength and it is thought this is linked to space weathering.

Polarimetry has not been as widely used for these purposes[13]. Ref. [14] shows that different solar panels can be characterized by their polarization in the lab. In this paper we aimed to test this on three GEO satellites.

This paper presents how the observations were made and calibrated in Section 2, then the results obtained in Section 3 and later a discussion and conclusions in Section 4.

2. METHODOLOGY

The study is based on satellite data collected at the Nordic Optical Telescope (NOT), is a 2.56 m telescope primarily used for astronomical research, located in the Roque de los Muchachos Observatory, in La Palma, Spain. Three geostationary satellites were chosen as targets for our observations; Intelsat 904, Intelsat 37e, and TDRS-13. The three satellites have been built on the same bus, but have been launched on different years to allow us to look for differences in their spectra that could be caused by space weathering (Intelsat 37e and TDRS-13 as they were launched in 2017, while Intelsat 904 was launched in 2002). In order to study how the polarimetry and spectroscopy changed

Table 1: Satellite observations with the Nordic Optical telescope[1].

Date:	Satellite:	Polarimetry (angles)	Spectroscopy (angles)	Comments:
2021-04-05	Intelsat 37e	3	-	Variable cloud coverage
	TDRS-13	2	-	
2021-05-05	Intelsat 37e	4	3	Problems with pointing the telescope
2021-06-27	Intelsat 37e	6	6	Good conditions
	Intelsat 904	6	6	
2022-04-11	Intelsat 37e	1	3	Variable cloud coverage part of the night
	TDRS-13	3	3	
	Inteslsat 904	1	1	

over phase angle with respect to the sun we observed the satellites on a variety of different phase angles and on a number of different dates to minimize systematic errors in the calibration. Table 2 shows the number of observations taken of each satellite on the different dates for both polarimetry and spectroscopy. All polarimetry observations were performed in the V-band.

The observational conditions varied between the campaign dates. Some dates experienced variable cloud coverage and required additional care in calibration in order to be used. From the observations taken, 20% could not be sufficiently calibrated. Since observing fast moving objects, such as satellites, had not been previously performed with the telescope the first few nights there were technical difficulties maintaining the object within the slit throughout the exposure time for spectroscopy. This was later fixed and high signal-to-noise spectra could be obtained. Some data had to be discarded on nights with variable cloud coverage when not all four polarimetry angles could be observed with good conditions for a single phase angle. The measurements were repeated on several separate nights in order to ensure consistency and allowed us to measure any potential systematic error to the calibration between measurements of different nights.

2.1 Linear polarimetry with FAPOL instrument

Polarimetry was taken using the FAPOL linear polarimeter in the Alhambra Faint Object Spectrograph and Camera (ALFOSC) at NOT. FAPOL utilizes a half-wave plate and a calcite plate mounted in the aperture wheel for and for our observations we used four angles, 0°, 22.5°, 45°, and 67.5°. Since the calcite plate allows simultaneous measurement of the both the ordinary and extraordinary component of the two polarized beams we get two images of the same object separated by approximately 15" on the image plane on each image taken. This separation is adequate for point-like sources. The beam-splitting from the calcite plate combined with the four positions of the half-wave plate means that eight images are obtained in total. The images have a near circular field of view of ≈ 1.1' which means that the target is often isolated and easy to identify.

The percentage of polarization for each angle is obtained as follows: Let O_i and E_i be the intensities of the ordinary and extraordinary images obtained through the calcite plate for each of the i=1,2,3,4 angles of the half-wave plate.

The percentage of linear polarization (P) is found as follows:

$$Q_i = E_i/O_i \tag{1}$$

$$QM = Q_1 + Q_2 + Q_3 + Q_4 \tag{2}$$

$$PX = \frac{Q_1 - Q_3}{QM} \tag{3}$$

$$PY = \frac{Q_2 - Q_4}{QM} \tag{4}$$

$$P = 100\sqrt{(PX)^2 + (PY)^2} \tag{5}$$

[1]The angles referred to in the table represent clusters of data points at similar phase angles. When possible, both polarimetry and spectroscopy have been performed for similar angles.

while the error is given by

$$\Delta P = \sqrt{\sum_{Q_i} \left(\frac{\partial P}{\partial Q_i} \Delta Q_i \right)^2}. \tag{6}$$

The calibration of the polarimetry images and spectra were performed according to standard procedure in astronomy using a custom made pipeline based on the Astropy [15] [16] python library. The calibration is described in more detail in Sections 2.2 and 2.3.

2.2 Calibration of polarimetry

All images were first bias and flat subtracted before aperture photometry could be used to extract the intensity of each image. The target source is identified with the "DAOStarFinder" algorithm in Astropy [17] which is more robust than the IRAF alternative. The sources are filtered to only keep pairs that are almost the same height and approximately 15" apart, corresponding to the ordinary and extraordinary beams. To estimate the background noise we draw an annulus with an inner radius of 1.4 times the full width at half maximum (FWHM) of the source to avoid source contamination, and the outer radius is adjusted so that the annulus area matches that of the inner ring. The brightness of the object is the difference between the measured aperture photometry and estimated background. The error is then estimated as the square root of the sum of the squares of the errors for both values.

Once all sources have been extracted, we employ Equation 5 to calculate the percentage of linear polarization for each object. Similar observations are also performed on solar analogue high precision polarimetry standard stars [18] with no polarization in order to have a zero polarimetry comparison to calibrate the data. Polarization calibration is performed to mitigate the effect of the atmosphere on the measured polarization.

2.3 Calibration of spectra

The spectroscopy images are first bias-corrected. In order to remove teluric emissions, we compute mean and variance of the image for each wavelength, excluding the object itself. Then, we create a new image the same size as the original filled with Gaussian noise where each row has the same mean and standard deviation as the original. This image is used as a dark frame in the reduction pipeline, hence dubbed "synthetic dark". In order to avoid some hot pixels across the edges, the synthetic dark ignores a band of 10 pixels from each edge. The flux is computed averaging across the rows of the image.

In order to obtain the wavelength calibration, we manually annotated 11 peaks from an observation of a Helium-Neon lamp, see Fig. 1. This gives us an approximate solution, but it doesn't account for effects like flex of the instrument with positioning, or thermal expansion. To compensate, each image is then automatically refined using a reference lamp spectrum taken shortly before or after the science image and it is compared with the NIST Atomic Spectra Database Lines [19].

The calibration algorithm takes the reference image that was taken closest in time to our exposure and proceeds. In the first step, we estimate the intensity of the continuum by taking a 21 pixel rolling median, to which we fit a Chebyshev polynomial of order 5. Then, we divide the spectrum by the fitted continuum, making the lines more prominent. We use the peak-finding algorithm `signal.find_peaks` from Scipy [20] to extract a list of possible candidates, sorted by intensity. We iterate over the peaks, and for each one, we find the strongest peak in the reference spectrum within a window of 90 Å. Whenever we find a peak, we verify that the match is plausible, ie, it is consistent with a monotonous wavelength solution. The pair is saved, and the matched peak is removed from the reference spectra to prevent it from being matched again.

Finally, we fit all pairs to a Gaussian process with a kernel that is the sum of a linear and a radial basis function. The first component of the kernel is responsible for the overall trend, while the second accounts for any deviation. This method provides both a robust estimate of the wavelength solution as well as an uncertainty based on the position of the lines. A summary of the calibration of the spectra is shown in Fig. 1 in schematic format.

3. RESULTS

Fig. 2 shows all the polarimetry measurements with respect to the phase angle. The phase angle is the angle between the direction of the Sun and the observatory as observed from the satellite; or in other words, the angle between the

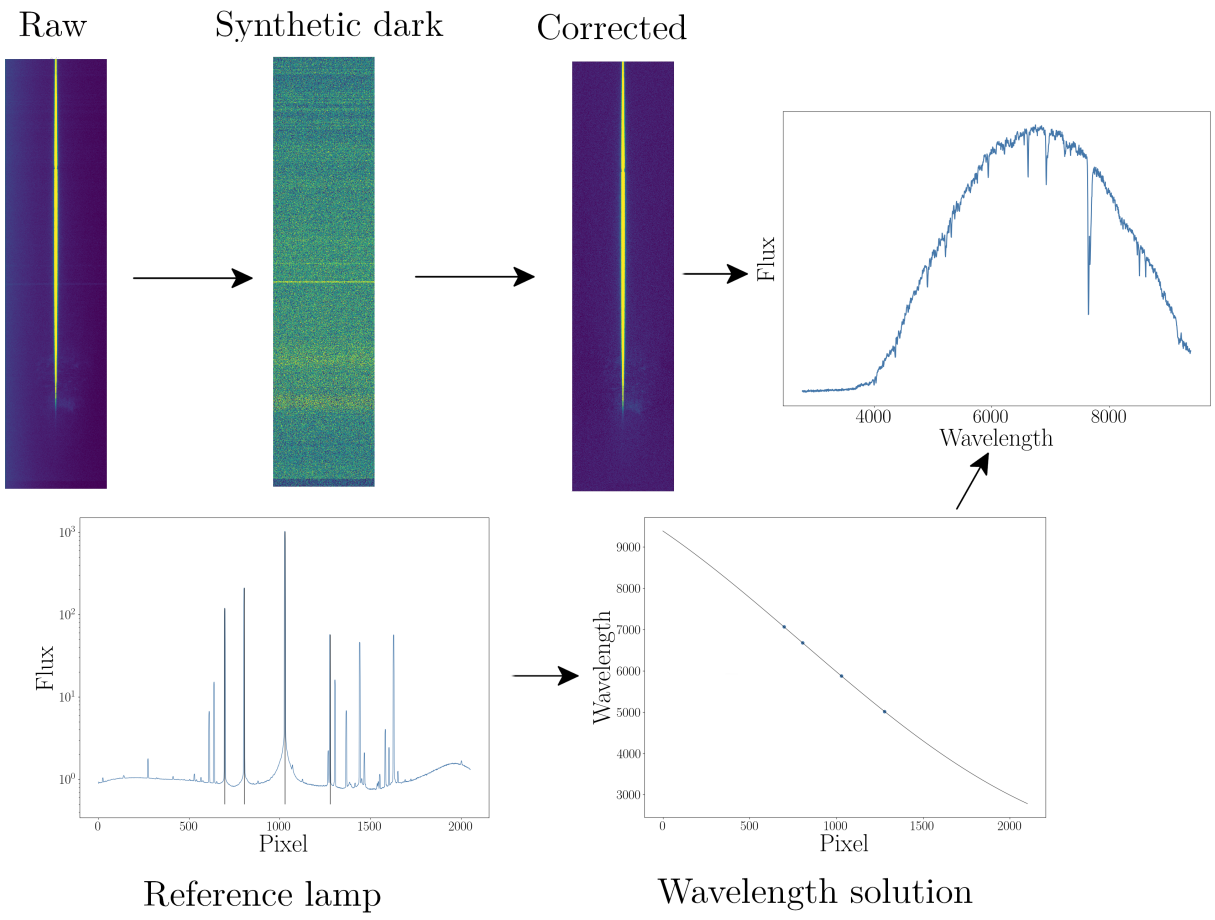

Fig. 1: A schematic showing the calibration steps for the spectra taken with the NOT from the raw spectra to the fully wavelength calibrated end product.

incident light and that reflected towards the telescope. The signed phase angle has the same magnitude, with the sign of the angle resulting from projecting the three objects into the Solar System plane in the International Celestial Reference System (ICRF) reference frame, and going from the Sun to the telescope. Mathematically, the angle is positive if the cross product of the vectors from the satellite to the Sun and the Earth points upwards in the Solar System plane.

They are fitted with a polynomial of order 3 to guide the eye and we find that the three satellites have distinct signatures, especially at large angles. For all satellites we also note that the polarization is not symmetric for the sign of the phase angle.

The variation between polarimetry measurements across different nights are showcased in Fig. 3 where we find relatively robust results despite the varying observational conditions.

For the spectra we found that the position of the peak and the shape of the spectrum vary, sometimes rapidly, and independent of physical characteristics such as phase angle. This variation suggest that a single spectrum may not be sufficient for characterization of unknown satellites. We also report rapid spectroscopical changes, up to a 20% decrease in flux in the near-infrared I band in two minutes, under good weather conditions. In Fig. 3 we show the spectra taken of Intelsat 37e and show the variation in both counts and peak wavelength observed. These variations in the peak wavelength are not observed for Intelsat 904. For TDRS-13 we have too few spectra to draw any conclusions.

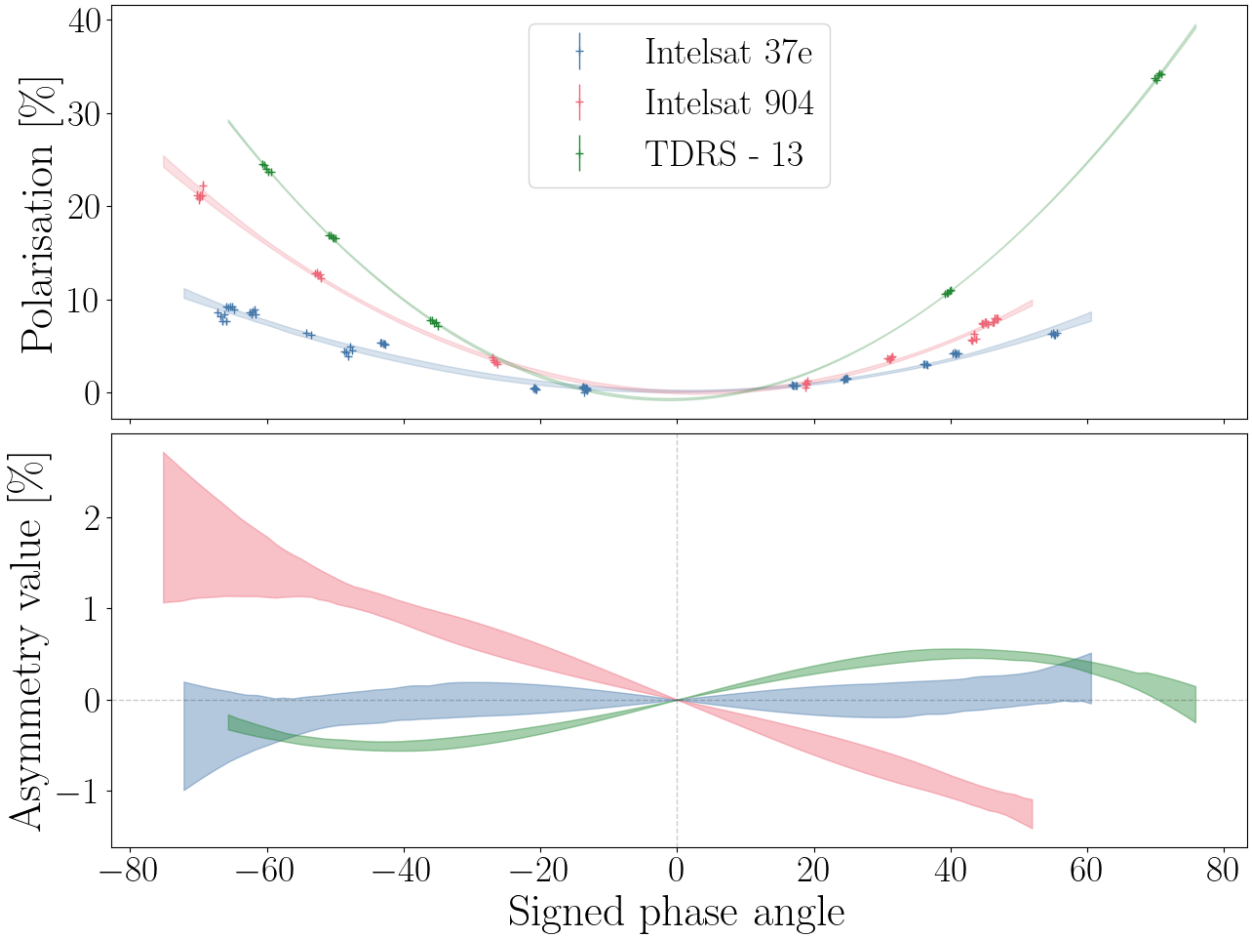

Fig. 2: The upper panel shows the polarization as a function of the signed phase angle for the three observed satellites. The shaded lines show a polynomial fit of order 3 and its 90% confidence interval, in order to guide the eye to differences in the polarization signature between the three satellites. Errorbars of 1 σ are shown however for some cases these are smaller than the markers used. The lower panel shows the asymmetry value, i.e. the asymmetric components of the fitted polynomial, for each satellite with respect to the signed phase angle. All three satellites show different characteristics.

4. DISCUSSION AND CONCLUSION

The observed difference in polarization between the satellites suggests that polarization could potentially be used as a cost-effective means for non-resolved object characterization. Since the polarization directly depends on the surface properties of the satellite, variation in polarization could also be used together with modeling to determine information about the configuration of the solar panels and antennas. Polarimetry only requires relatively short exposure times, which makes such observations relatively accessible for low-end instrumentation and viable for large-scale studies. This is especially important for reaching a better understanding of object characterization in an even more crowded space environment, as large number of objects may need to be characterized. In addition, the method also seems robust across several nights in varying observing conditions. Further work is needed to corroborate this and to quantify the variation and phase angle dependence.

Further work could expand the measurements to a larger number of satellites and include modeling of the object geometry to see how it is linked to the polarization, as well as an investigation of how stable the signature is over time. It is encouraging that the polarimetry signatures are very distinct, but it it should be noted that we only look at three objects in this paper, a larger study is required to reach broader conclusions on the potential of polarimetry

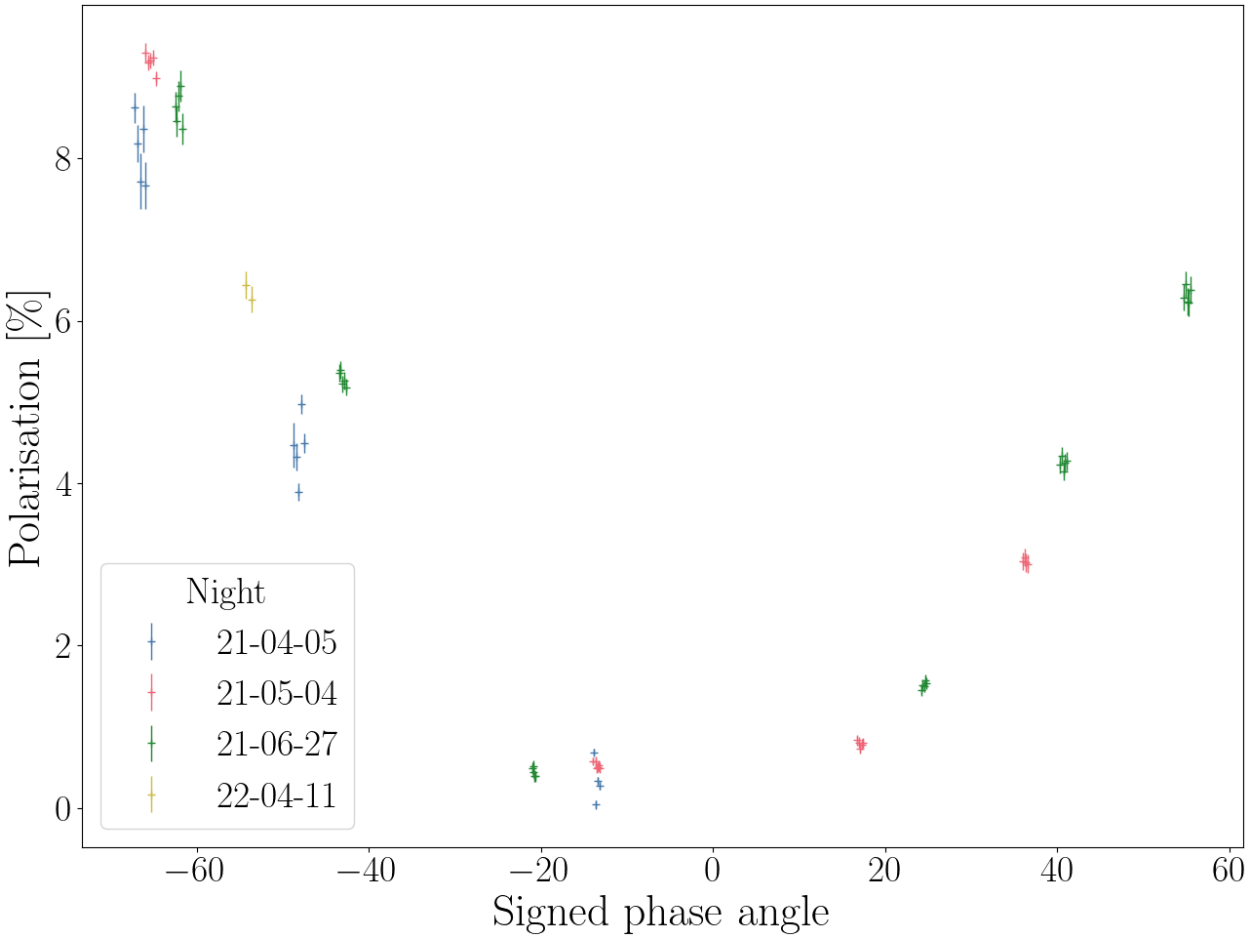

Fig. 3: Polarimetry observations of Intelsat 37e divided by their observation date. Errorbars of 1 σ are shown however for some cases these are smaller than the markers used.

measurements in non-resolved object characterization.

Combining polarimetry with photometry would possibly allow an inference of the 3D shape of the object with help of computer modeling. Combining different methods of different observations, such as light curves to get further characterization information of the RSO has been done before with promising results. Ref. [21] offer a mass estimation method using astrometric and photometric data fusion of RSOs. Others studies, such as [22] explore methods to estimate the albedo-area for stable GEO RSOs.

The peak intensity shift found on the spectra from Intelsat 37e require further research in order to ascertain its cause. Confounding factors may include cloud coverage and differences in the solar panel composition, which makes it difficult to draw firm conclusions for the origin of the spectral differences and changes. Further studies aimed to study reddening due to space weathering would thus require observations at several phase angles. In addition, identical satellites launched at different times should be used to minimize additional confounding factors.

5. ACKNOWLEDGMENTS

The data presented here were obtained with ALFOSC, which is provided by the Instituto de Astrofisica de Andalucia (IAA) under a joint agreement with the University of Copenhagen and NOT. Special thanks to Anlaug Amanda Djupvik at the NOT who helped with the observations.

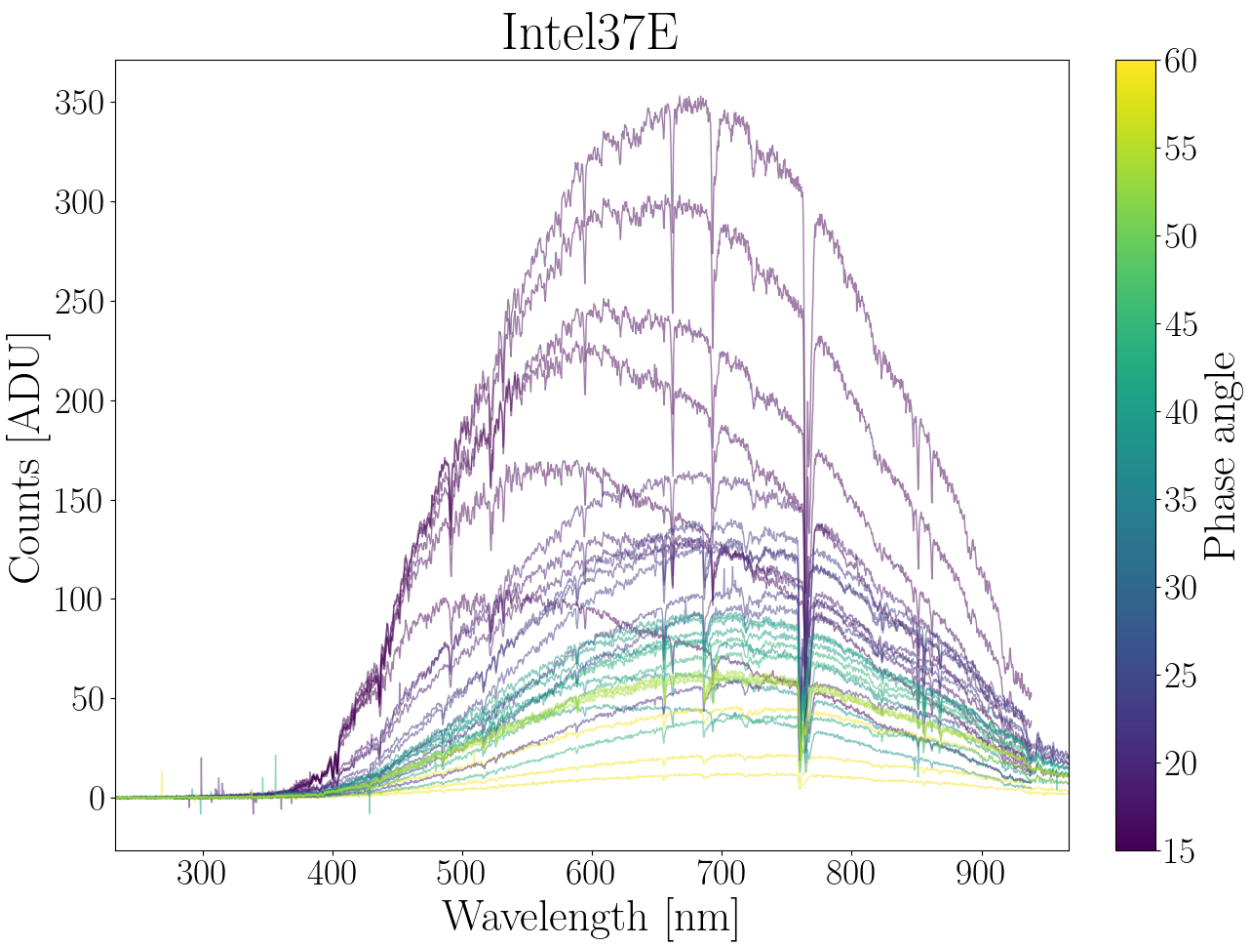

Fig. 4: All the spectra taken of Intelsat 37e, color-coded by phase angle.

6. REFERENCES

[1] B Weeden, P Cefola and S. Jaganath Global space situational awarenss sensors *Proc. of Maui Optical and Space Surveillance Technologies Conf.*, Maui, Hawaii, (2010)

[2] T E.Payne, S A. Gregory, and K Luu SSA Analysis of GEOS Photometric Signature Classifications and Solar Panel Offsets *Advanced Maui Optical And Space Surveillance (AMOS) Technologies Conference* (2006)

[3] E Kerr, E G. Petersen, P Talon, D Petit, C Dorn and S Eves Using AI to Analyse Light Curves for GEO Object Characterisation *Advanced Maui Optical And Space Surveillance (AMOS) Technologies Conference* (2021)

[4] R Furfaro, R Linares and V Reddy Space debris identification and characterization via Deep meta-learning First International Orbital debris conference (2019)

[5] Jorgensen, K., Africano, J., Hamada, K., Stansbery, E., Sydney, P. & Kervin, P. Physical properties of orbital debris from spectroscopic observations. *Advances In Space Research*. **34**, 1021-1025 (2004)

[6] Seitzer, P., Lederer, S., Cowardin, H., Barker, E. & Abercromby, K. Visible light spectroscopy of GEO debris. *13th Annual Advanced Maui Optical And Space Technical Conference*. (2012)

[7] Bedard, D. & Wade, G. Time-resolved visible/near-infrared spectrometric observations of the Galaxy 11 geostationary satellite. *Advances In Space Research*. **59**, 212-229 (2017)

[8] http://www.not.iac.es/instruments/alfosc/polarimetry/linpol.html, NOT webpage, accessed 2022-08-23

[9] Vananti, A., Schildknecht, T. & Krag, H. Reflectance spectroscopy characterization of space debris. *Advances In Space Research*. **59**, 2488-2500 (2017,5)

[10] A Battle, V Reddy, R Furfaro, T Cambell, J Frith and D Monet A visible spectral atlas of geostationary satellites *Advanced Maui Optical And Space Surveillance (AMOS) Technologies Conference* (2021)

[11] JorgensenAbercromby, K., Hamada, K., Okada, J., Guyote, M. & Barker, E. Comparisons of Ground Truth and Remote Spectral Measurements of the FORMOSAT and ANDE Spacecrafts. *AMOS 2006 Conference*. (2006)

[12] Abercromby, K., Guyote, M., Okada, J. & Barker, E. Applying space weathering models to common spacecraft materials to predict spectral signatures. *2005 AMOS Technical Conference*. (2005)

[13] R Swindle, J Gazak, M Phelps, I McQuaid and J Fletcher Learned satellite identification using low-resolution spectropolarimetry. *Polarization: Measurement, Analysis, And Remote Sensing XV*. **12112** pp. 121120H (2022)

[14] Beamer, D., Abeywickrema, U. & Banerjee, P. Polarization vector signatures for target identification. *Society Of Photo-Optical Instrumentation Engineers (SPIE) Conference Series*. **10407** pp. e104070T (2017,8)

[15] Astropy Collaboration, Robitaille, T., Tollerud, E., Greenfield, P., Droettboom, M., Bray, E., Aldcroft, T., Davis, M., Ginsburg, A., Price-Whelan, A., Kerzendorf, W., Conley, A., Crighton, N., Barbary, K., Muna, D., Ferguson, H., Grollier, F., Parikh, M., Nair, P., Unther, H., Deil, C., Woillez, J., Conseil, S., Kramer, R., Turner, J., Singer, L., Fox, R., Weaver, B., Zabalza, V., Edwards, Z., Azalee Bostroem, K., Burke, D., Casey, A., Crawford, S., Dencheva, N., Ely, J., Jenness, T., Labrie, K., Lim, P., Pierfederici, F., Pontzen, A., Ptak, A., Refsdal, B., Servillat, M. & Streicher, O. Astropy: A community Python package for astronomy. *Astronomy & Astrophysics*. **558** pp. eA33 (2013,10)

[16] Astropy Collaboration, Price-Whelan, A., Sipocz, B., Gunther, H., Lim, P., Crawford, S., Conseil, S., Shupe, D., Craig, M., Dencheva, N., Ginsburg, A., Vand erPlas, J., Bradley, L., Pérez-Suárez, D., De Val-Borro, M., Aldcroft, T., Cruz, K., Robitaille, T., Tollerud, E., Ardelean, C., Babej, T., Bach, Y., Bachetti, M., Bakanov, A., Bamford, S., Barentsen, G., Barmby, P., Baumbach, A., Berry, K., Biscani, F., Boquien, M., Bostroem, K., Bouma, L., Brammer, G., Bray, E., Breytenbach, H., Buddelmeijer, H., Burke, D., Calderone, G., Cano Rodríguez, J., Cara, M., Cardoso, J., Cheedella, S., Copin, Y., Corrales, L., Crichton, D., D'Avella, D., Deil, C., Depagne, É., Dietrich, J., Donath, A., Droettboom, M., Earl, N., Erben, T., Fabbro, S., Ferreira, L., Finethy, T., Fox, R., Garrison, L., Gibbons, S., Goldstein, D., Gommers, R., Greco, J., Greenfield, P., Groener, A., Grollier, F., Hagen, A., Hirst, P., Homeier, D., Horton, A., Hosseinzadeh, G., Hu, L., Hunkeler, J., Ivezic, Z., Jain, A., Jenness, T., Kanarek, G., Kendrew, S., Kern, N., Kerzendorf, W., Khvalko, A., King, J., Kirkby, D., Kulkarni, A., Kumar, A., Lee, A., Lenz, D., Littlefair, S., Ma, Z., Macleod, D., Mastropietro, M., McCully, C., Montagnac, S., Morris, B., Mueller, M., Mumford, S., Muna, D., Murphy, N., Nelson, S., Nguyen, G., Ninan, J., Nothe, M., Ogaz, S., Oh, S., Parejko, J., Parley, N., Pascual, S., Patil, R., Patil, A., Plunkett, A., Prochaska, J., Rastogi, T., Reddy Janga, V., Sabater, J., Sakurikar, P., Seifert, M., Sherbert, L., Sherwood-Taylor, H., Shih, A., Sick, J., Silbiger, M., Singanamalla, S., Singer, L., Sladen, P., Sooley, K., Sornarajah, S., Streicher, O., Teuben, P., Thomas, S., Tremblay, G., Turner, J., Terrón, V., Van Kerkwijk, M., De la Vega, A., Watkins, L., Weaver, B., Whitmore, J., Woillez, J., Zabalza, V. & Astropy Contributors The Astropy Project: Building an Open-science Project and Status of the v2.0 Core Package. *The Astrophysical Journal*. **156**, e123 (2018,9)

[17] Stetson, P. DAOPHOT: A Computer Program for Crowded-Field Stellar Photometry. *Publications of the Astronomical Society of the Pacific*. **99** pp. 191 (1987,3)

[18] V Piirola, A Berdyugin, P C. Frisch, M Kagitani, T Sakanoi, S Berdyugina, A A. Cole, C Harlingten and K Hill High-precision polarimetry of nearby stars (d<50pc) *Astronomy & Astrophysics*, 635, A46, 2020

[19] Kramida, A. & Ralchenko, Y. NIST Atomic Spectra Database, NIST Standard Reference Database 78., National Institute of Standards, (2021)

[20] Virtanen, P., Gommers, R., Oliphant, T., Haberland, M., Reddy, T., Cournapeau, D., Burovski, E., Peterson, P., Weckesser, W., Bright, J., Van der Walt, S., Brett, M., Wilson, J., Millman, K., Mayorov, N., Nelson, A., Jones, E., Kern, R., Larson, E., Carey, C., Polat, İ., Feng, Y., Moore, E., VanderPlas, J., Laxalde, D., Perktold, J., Cimrman, R., Henriksen, I., Quintero, E., Harris, C., Archibald, A., Ribeiro, A., Pedregosa, F., Van Mulbregt, P. & SciPy 1.0 Contributors SciPy 1.0: Fundamental Algorithms for Scientific Computing in Python. *Nature Methods*. **17** pp. 261-272 (2020)

[21] V Mallik and M Jah Reconciling space object observed and solar pressure albedo-areas via astrometric and photometric data fusion. *Advances In Space Research*. **63**, 404-416 (2019,1)

[22] Payne, T., Gregory, S., Dentamaro, A., Ernst, M., Hollon, J., Kruchten, A., Chaudhary, A. & Dao, P. Development and Evaluation of New Methods for Estimating Albedo-area for Stable GEOs. *Advanced Maui Optical And Space Surveillance (AMOS) Technologies Conference*. pp. e24 (2017,1)